Nonlinear Model Predictive Control for Mitigating Epidemic Spread using a Partial Differential Equation Based Compartmental Dynamic Model

Logan Street * Deepak Antony David * Chunyan Liu **
Shelley Ehrlich ** Manish Kumar *
Subramanian Ramakrishnan ***

* Department of Mechanical and Materials Engineering, University of Cincinnati, Cincinnati, OH, USA. email: streetln@mail.uc.edu, daviddy@mail.uc.edu, kumarmu@ucmail.uc.edu

** Cincinnati Children's Hospital Medical Center, Division of Biostatistics and Epidemiology, University of Cincinnati College of Medicine, OH, USA. email: chunyan.liu@cchmc.org, shelley.ehrlich@cchmc.org

*** Department of Mechanical and Aerospace Engineering, University of Dayton, Dayton OH, USA. email: sramakrishnan1@udayton.edu

Abstract: We present a Nonlinear Model Predictive Control (NMPC) framework for epidemic spread mitigation using a Partial Differential Equation (PDE) based Susceptible-Latent-Infected-Recovered (SLIR) epidemiological dynamic model. The spatio-temporal epidemic spread predictions of the model were numerically validated in our previous work using empirical COVID-19 data for Hamilton County, Ohio, employing a single-objective Genetic Algorithm (GA) for training model parameters. The validated model serves as the basis for the NMPC prediction and control framework developed to support the design of optimal Non-Pharmaceutical Interventions for spread mitigation. We consider a cost function comprising the infection spread density and the cost of applied control, with the latter representing socioeconomic effects. With a prediction horizon (T_p) of 30 days and a control horizon (T_u) of 15 days. The NMPC investigates a uniformly distributed control scheme across the entire spatial domain for three different time periods of the COVID-19 pandemic with distinct infection trends. In summary, the article presents one of the first efforts towards developing an NMPC framework based on a spatio-temporal epidemic dynamic model. The results provide an analytical basis for improved spread mitigation of future epidemics.

Keywords: Nonlinear Model Predictive Control, Partial Differential Equations, Mathematical Modeling, Epidemic Models, Numerical Analysis, Numerical Optimization.

1. INTRODUCTION

The COVID-19 pandemic had a major impact globally with the first cases occurring in Wuhan, China. As seen from the Center for Disease Control's Museum COVID-19 Timeline CDC (2023), the infections began to spread rapidly and soon COVID-19, caused by the virus SARS-COV-2, was expanding globally at an alarming rate. In response, Non-Pharmaceutical Interventions (NPIs) such as social distancing, travel restrictions, masking, and lockdowns in various degrees were implemented across the globe, even as intense efforts were focused on developing

pharmaceutical countermeasures including vaccine development. However, the lead time essential to develop effective pharmaceutical interventions underscores the criticality of NPI for effective spread mitigation, particularly in the early stages of a novel epidemic. An epidemic is indeed a complex dynamic system; therefore it is significant to consider NPI as control interventions aimed at driving an epidemic to lower infection states and seek to develop NPI based on control-theoretic analysis based on available empirical infection spread data. This viewpoint fundamentally motivates the research reported in this paper.

Real-world epidemics are characterized by spatio-temporal dynamics for which partial differential equations (PDE) provide a more accurate representation (Mandal et al. (2020); Yang et al. (2014)). Specifically, reaction-diffusion type PDE are useful for studying the coupled, spatio-temporal dynamics of multiple interacting entities, as evident in other applications (Deshpande et al. (2017); Wang

^{*} This work was supported by the National Science Foundation [Grant Numbers- 2140405 (PI - Ramakrishnan), 2140420 (PI - Kumar), and 2140441 (PI - Ehrlich)]. We would like to express our gratitude to Greg Kesterman (the Hamilton County Health Commissioner), David Carlson, and Nathan Williams of The Epidemiology Division of Hamilton County Public Health for providing the essential data that served as a cornerstone for this study.

et al. (2012)). We also note here our previous work on epidemic spread prediction using a PDE model, validated using COVID-19 data from Ohio (Majid et al. (2021, 2022)). Yet another important classification is between deterministic and stochastic epidemic models. Uncertainties arising from human behavior, the environment, and pathogen transmission, all influence epidemic dynamics pointing to the significance of stochastic models, including the use of fractional stochastic differential equations (Atangana and İgret Araz (2022)). Approaches such as agent-based modeling (Maziarz and Zach (2020); Shamil et al. (2021); Truszkowska et al. (2021)), as well as machine learning techniques (Mehta et al. (2020)) have also been used in epidemic dynamics in the COVID-19 context.

Turning next to control, several papers have discussed Model Predictive Control (MPC) for COVID-19 spread mitigation, using ODE frameworks (Carli et al. (2020); Köhler et al. (2021); Scarabaggio et al. (2022); Morato et al. (2022); Armaou et al. (2022)). While MPC based on PDE frameworks have been reported in the context of applications, for instance, (Wang and Yamamoto (2020); Dufour et al. (2004); Dietze and Grepl (2023)), this remains much less explored - particularly in the context of epidemic control - and motivates our effort in this paper. The primary contribution of this paper is to develop and implement a Nonlinear Model Predictive Control (NMPC) framework as a mathematical and computational tool capable of determining control actions that optimize a cost function accounting for infection spread intensity as well as the socioeconomic costs of the applied control. The approach employs our previously developed and validated PDE-based SLIR model that captures the spatiotemporal dynamics of epidemic spread (Majid et al. (2021, 2022)), allowing us to implement the control in spatial and temporal granularity of our choice.

In Section 2, we discuss the mathematical modeling of the SLIR PDE, the parameters implemented within the model, the NMPC framework, and the implemented control scheme. An evaluation of the model using empirical COVID-19 data for Hamilton County, Ohio is analyzed in Section 3 along with the results obtained from the NMPC simulations. Discussions around these results are also presented. The conclusions from this research as well as an outlook for further work are presented in Section 4.

2. MATHEMATICAL MODELING AND THE NMPC FRAMEWORK

2.1 Partial Differential Equation Based SLIR Model

We begin by reiterating that the present effort builds upon our previous work reported in (Majid et al. (2021, 2022)) that focused on developing and validating a PDE-based SLIR modeling framework. The non-dimensional compartmental model equations are:

$$\frac{\partial S}{\partial t} = \lambda + \eta_S \nabla^a S - \theta S - u(x, y, t) \phi IS \tag{1}$$

$$\frac{\partial L}{\partial t} = \eta_L \nabla^a L + u(x, y, t) \phi IS - u(x, y, t) \epsilon \phi \qquad (2)$$

$$\times \left(\int_{-\infty}^{\infty} \int_{-\infty}^{\infty} I(x, y, t - \tau) S(x, y, t - \tau) f_a(x, y) dx dy \right)$$

$$\frac{\partial I}{\partial t} = \eta_I \nabla^a I - \delta I + u(x, y, t) \epsilon \phi \tag{3}$$

$$\times \left(\int_{-\infty}^{\infty} \int_{-\infty}^{\infty} I(x, y, t - \tau) S(x, y, t - \tau) f_a(x, y) dx dy \right)$$

$$\frac{\partial R}{\partial t} = \eta_R \nabla^a R - \theta R + \omega I \tag{4}$$

Where,

 λ - Birth rate in the domain.

 η_S - Diffusion coefficient representative of intensity of the random motion of the susceptible population.

 η_L - Diffusion coefficient representative of intensity of the random motion of the latent population.

 η_I - Diffusion coefficient representative of intensity of the random motion of the infected population.

 η_R - Diffusion coefficient representative of intensity of the random motion of the recovered population.

 ∇^a - Laplacian operator to represent the random motion of the PDEs. Please note that throughout this work Brownian motion is considered. As such the diffusion operator a=2 is applied.

au - The period of latency between compartments.

 θ - Mortality rate due to natural deaths.

 ϕ - Infection rate.

 δ - Removal of individuals from the infected compartment due to death or recovery.

 ϵ - Fraction of the infected population that survive the latency period and enter the infected category.

u(x, y, t) - The control parameter which is a function of space and time.

 $f_a(x, y)$ - Gaussian kernel defining the extent of the mobility of the latent population.

Some observations about the model equations are in order here. Firstly, we note that the coupling term in PDE for S, i.e. that last term in Eq. 1, represents the transition from the S to the Latent L compartment. A key point is that the control u(x, y, t) is applied to this term. Secondly, that the PDE system is of the reaction-diffusion type naturally affords a probabilistic interpretation of the dynamics if one considers the compartmental densities as probability densities. In other words, the system of PDEs may be considered similar to the Fokker-Planck type equations invoked in stochastic dynamics. Finally, we note that to obtain the parameters of the above SLIR equations, we utilized a single-objective Genetic Algorithm (GA) following a similar approach used by (Yarsky (2021); Torlapati and Clement (2019)). The GA finds the parameters of the above model that minimizes the error between the model outputs versus the ground truth data (in this case, COVID-19 data for Hamilton County, OH).

2.2 NMPC Framework and Methods of Control

The NMPC framework follows a closed-loop control scheme. The approach utilizes the PDE-based SLIR model presented in Eqs. 1 - 4, the parameters of which can be trained using real-world epidemic data. Once this training and initialization of the PDE states is completed, the NMPC then begins its evaluation process where it considers the control to be active. The approach determines the control action that optimizes a specified cost function. The PDE-based SLIR model is used to evaluate the cost function based on the application of a control action over a specified prediction horizon. The optimal control action

thus obtained is then applied for the length of our control horizon. After this period, the process then begins again for the period of our choosing.

For evaluating the model control was uniformly distributed across the models environment. The numerical value of the control action in the model given by equations 1-4 is denoted as u and is bounded as: $0 \le u \le 1$. For computational ease and also accounting for the fact that NPI measures are discrete in practice, we consider the control to be varying with the step size 0.1. In other words, u belongs to a vector given by: u = [0, 0.1, 0.2, ...1]. This allows the control action to potentially take on 11 different possible values each theoretically representing discrete types of NPI measures.

We note that u is a multiplication factor in Eq. 1 affecting the conversion of the susceptible population to the latent population, and eventually to the infected population. The control action u=1 signifies that no control is applied; correspondingly it allows maximum conversion. On the other hand, u=0 represents the strictest control scenario such as a complete lockdown that does not allow any conversion. The value that u takes on is applied as a constant within the SLIR compartment/state equations for the total length of the control horizon. To determine the optimal control value that should be implemented for when control is applied uniformly, we consider the following cost function:

$$J(u) = I_{Final}^{T_p}(u) + W(1-u)^2$$
 (5)

Where,

u - Control action.

W - Weight factor applied to the control action (u). $I_{Final}^{T_p}(u) = \int \int I(x, y, T_p) dx dy$.

The cost function given by Eq. 5 is straightforward as the main focus is to minimize the infection while penalizing the control action. The $I_{Final}^{T_p}(u)$ term represents the total number of infected people at the end of the prediction horizon T_p , obtained under control action u applied constantly for the entire prediction horizon. The weight factor W is a parameter that incorporates the cost of control in the overall cost function. Note the term (1-u) signifies that a smaller value of u implies stricter control and hence needs to be penalized more. Indeed, choosing the value of W based on a deeper analysis of socioeconomic impacts from NPI measures would be ideal; however, that is beyond the scope of the current paper and is in the realm of future work.

3. RESULTS AND DISCUSSIONS

3.1 Hamilton County, Ohio Case Study

In this paper, the environment used for the application of the SLIR state equations and the proposed NMPC approach is that of Hamilton County, Ohio. The dataset that we have utilized contains the true infection and death data based on the zip codes that make up Hamilton County. The whole spatial domain is discretized into a 60 by 60 cell grid covering an area of approximately 413 square miles. The SLIR state equations are also discretized by applying Euler's forward method. The resulting non-dimensional/discretized SLIR equations are as follows (Maiid et al. (2021, 2022)):

$$S_{x,y}^{T+1} = N\lambda + \eta_S (S_{x,y+1}^T + S_{x,y-1}^T + S_{x+1,y}^T + S_{x-1,y}^T) + (1 - 4\eta_S - \theta - u \frac{\phi}{N} I_{x,y}^T) S_{x,y}^T$$
(6)

$$L_{x,y}^{T+1} = \eta_L (L_{x,y+1}^T + L_{x,y-1}^T + L_{x+1,y}^T + L_{x-1,y}^T) + (1 - 4\eta_L) L_{x,y}^T + \frac{\phi}{N} I_{x,y}^T S_{x,y}^T - \epsilon \frac{\phi}{N} \sigma_{x,y}^T$$

$$I_{x,y}^{T+1} = \eta_I (I_{x,y+1}^T + I_{x,y-1}^T + I_{x+1,y}^T + I_{x-1,y}^T)$$
(7)

$$I_{x,y}^{T+1} = \eta_I (I_{x,y+1}^T + I_{x,y-1}^T + I_{x+1,y}^T + I_{x-1,y}^T) + (1 - 4\eta_I - \delta) I_{x,y}^T + \epsilon u \frac{\phi}{N} \sigma_{x,y}^T$$
(8)

$$R_{x,y}^{T+1} = \eta_R (R_{x,y+1}^T + R^T x, y - 1 + R_{x+1,y}^T + R_{x-1,y}^T) + (1 - 4\eta_R - \theta) R_{x,y}^T + \omega I_{x,y}^T$$
(9)

$$\sigma_{x,y}^{T+1} = \sum_{i=1}^{n} \sum_{j=1}^{n} I_{x,y}^{T-\tau} S_{x,y}^{T-\tau} f_a l^2$$
 (10)

$$f_a(x,y) = \frac{1}{\sqrt{4\pi\alpha}} e^{-\frac{(i-x)^2 + (j-y)^2}{4\alpha}}$$
 (11)

Here, $X_{x,y}^{T+1}$ represents the values of compartments/states (S, L, I, or R) for a particular discrete location in (x,y) on the day T+1. σ represents the latent population for a discrete location on a specific day and the value is obtained from infected/susceptible states using Eq. 10. Here, τ is the latency period which represents the time taken for an individual to transition from the susceptible, latent, and lastly infected population once exposed to infection. The N term represents the total population corresponding to the area of interest. The f_a term represents a convolution kernel for representing the mobility of the latent population. Lastly, a Gaussian function is used to represent a diminishing probability of the latent population moving away from a specified location.

Within the 60 by 60 cells that are distributed across Hamilton County, we have considered a Neumann Boundary Condition. In the cells that may overlap with the boundary line or approach the boundary line, there is no migration of individuals across the boundary. If an attempt is made by an individual in the population to cross the boundary (due to diffusion terms in the model), it is simply redirected back. This allows us to conserve the population within the environment. Not all of the cells are directly in the true environment of Hamilton County and as such these cells do not contain this information but are still included. In total, there are 1383 cells that contain the actual environment space corresponding to the physical space in Hamilton County, Ohio. Additionally, we assume that an individual who has become infected is transitioned to the recovered population after a period of 21 days.

To demonstrate our proposed approach using real-world data, we consider three different time periods during the COVID-19 pandemic for Hamilton County, Ohio. The time periods are as follows: First (T1) = April 20, 2020, to June 3, 2020, Second (T2) = October 15, 2020, to December 28, 2020, and Third (T3) = February 15, 2021, to March 31, 2021. The time period (T1) provide insights into the influence of NMPC during the initial start of the lockdowns imposed in Hamilton County. We also note that around this time extreme countermeasures for mitigation were starting to be implemented across the United States in response to the initial wave of COVID-19 spread. The time period (T2) captures the start of the Alpha variant

of COVID-19. This variant began to spread in a super spreader type manner leading to a significant increase in infections across Hamilton County. By looking into the effects that the Alpha variant imposed we can get a greater understanding of the rapid dynamics that an infection of this manner can yield. Lastly, the time period (T3) allows us to observe the decline of infections following a dramatic increase that had occurred within Hamilton County prior. This observation is based on the publicly available empirical data. This transition period proves to be a point of interest as it allows us to address the dynamics while in a state of decay compared to that of a state of growth such as what occurred during the second time period (T2).

As discussed previously, in order to obtain the necessary parameters for the SLIR Eqs. 1 - 4 & 6 - 11 we have made use of a single-objective genetic algorithm. The reason we have chosen to utilize a GA for obtaining the parameters is because we found that in terms of computational time we saw greater performance compared to the original method used in Majid et al. (2021, 2022). The parameters that we have obtained from the GA for the three time periods (T1, T2, and T3) can be seen in Table. (1).

Table 1. Model Parameters

Parameters	(T1)	(T2)	(T3)
λ	0.0072	0.0308	0.0084
η_S	4.8818×10^{-5}	6.7088×10^{-4}	6.1000×10^{-5}
η_L	3.1601×10^{-5}	0.0816	2.9251×10^{-5}
η_I	1.8013×10^{-5}	0.0062	2.2501×10^{-5}
η_R	2.8900×10^{-5}	5.3970×10^{-8}	6.8410×10^{-5}
au	5 days	5 days	5 days
θ	5.7700×10^{-15}	2.8200×10^{-15}	2.8030×10^{-15}
φ	4.0284×10^{-4}	4.6908×10^{-4}	3.2884×10^{-4}
δ	0.0280	1.0002×10^{-5}	0.0280
ω	0.0283	0.0517	0.0490
ϵ	0.1353	0.1631	0.1500
α	0.8019	0.0029	0.6315

One of the first tasks is to obtain an appropriate value of weighting factor W in the cost function given by Eq. 5. It may be noted that total infections would be minimum when strictest control corresponding to u = 0 is applied. However, a strict control would have undesirable socioeconomic effect in the region. Since a detailed analysis of socioeconomic impact of different interventions is beyond the scope of this paper, we conducted a numerical evaluation of the cost function to determine a suitable value of W that would show demonstrable impact on the cost function. In this evaluation, we observed the values of W that would produce a convex curve for the total cost function signifying the fact that a feasible choice of control input exists where relative contribution of two terms in the cost function, infections and cost of control, would be properly weighted to have effect on the total cost value. We found an appropriate value of W to be 9500 that has been used in all of the simulations. In Fig. (1), an example of the analysis that we performed for the weight factor Wcan be observed.

In all the results presented as follows, we consider a prediction horizon of $T_p = 30$ days and control horizon of $T_u = 15$ days. This means that the cost function is evaluated for its value when prediction is carried out for 30 days from the current day considering a constant

application of control u for entire 30 days. This process is carried out at the interval of every 15 days which means a new value of optimal control action is obtained at every 15 days. In this paper, we present results for 2 succeeding applications of control actions at 15 day intervals each. We have considered the control horizon of 15 days since it provides a good time granularity in which interventions can be implemented in real-world. Also, a prediction horizon of 30 days was chosen since a larger value would result in erroneous prediction due to changing nature of the pandemic.

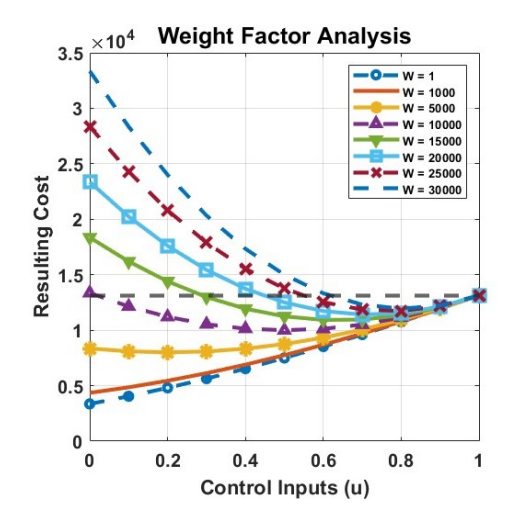


Fig. 1. Weight Factor Analysis

3.2 Simulation Processes

For each simulation, they follow the same steps. These steps include: training/initialization, prediction, optimization, and implementation. Where the prediction, optimization, and implementation are repeated depending on how many instances of applied control we are using. For each of the simulations, we have considered that the process is conducted two times (that represents the two instances of control applied). This implies that we carry out the optimization process twice with respect to the cost function Eq. 5. In each of numerical studies presented here, real-world data from day 0 to day 30 is used to train the parameters of the PDE-based SLIR model (please see Majid et al. (2021, 2022) for details on this approach). The first instance of control is applied from day 30 to day 45, and the second instance of control is applied from day 45 to day 60. In Fig. (2), we show the process that all of the simulations follow. For brevity, we present the full simulation process/results for the second time period (T2)

Figure (2) begins by showing the prediction of infected people based on the output of the PDE-based SLIR model. The model is trained using the real-world data from Day 0 - Day 30. Subsequently, 11 different plots showing infection numbers for 11 different potential values of u is shown for the prediction horizon $(T_p(1)=30 \text{ days}, \text{Day } 31 \text{ -Day } 60)$ for the 1st instance of control. Similarly, the next plot shows the model prediction for infection numbers for 11 different potential values of u for the prediction horizon $(T_p(2)=30 \text{ days}, \text{Day } 46 \text{ -Day } 75)$ for the 2nd instance of control. The figure also shows the model outputs as a result

of application of the first instance of control (u=0.50, obtained from optimization process) from Day 31 - Day 45. Lastly, the final plot shows the real-world infection numbers, model output when no control is applied (u=1), and when two instances of optimal controls (u=0.50 for both instances) are applied for the first control horizon ($T_u(1)$ from Day 31 - Day 45) and the second instance of the control horizon ($T_u(2)$ from Day 46 - Day 60).

Table 2. Simulation Results

Data Type	(T1)	(T2)	(T3)
Optimal Control (1)	u = 0.8	u = 0.5	u = 0.8
Optimal Control Cost (1)	2515	9874	3854
Optimal Control (2)	u = 0.8	u = 0.5	u = 0.8
Optimal Control Cost (2)	3288	8838	4411
Infections without Control	2840	13135	4343
Infections with Control	2135	7499	3474

3.3 (T1) - First Time Period

The results for the time period (T1) (please see Table. 2) indicate a total number of 2135 infections, in contrast to the 2840 infections observed in the absence of control, i.e., approximately a 25% reduction in new infections. The corresponding optimal control value was determined to be u=0.8 for both instances of control, where the cost of the first instance of control was 2515 and the cost of the second instance of control was 3288. Essentially, with respect to the empirical COVID-19 data the NMPC has determined that a moderate increase/application of control should be taken at this time. However, this result makes sense given that, at this time, the total number of infections were at a lower amount compared to other time periods.

3.4 (T2) - Second Time Period

The results for the time period (T2) (please see Table. 2) indicate a total number of 7499 infections when control is active on the environment. In the absence of control, the total number of infections was 13135. By applying control to the environment, we observed approximately a 43% reduction in infections. The corresponding optimal control value for both instances came out to be u = 0.5, where the cost of the first instance of control was 9874 and the cost of the second instance of control was 8838. As mentioned prior this time period is associated with the emergence of the Alpha variant of COVID-19 leading to an increase in infections as well as the total overall cost. Unlike the first time period (T1), the cost for second instance of control was lower than the cost for the first instance of control. This proves to be interesting as we can infer this as the control measure is achieving a steady level of containment for the infection.

3.5 (T3) - Third Time Period

The results for the time period (T3) (please see Table. 2) indicate a total number of 3474 infections when control is active on the environment. In the absence of control, the total number of infections was 4343. By applying control to the environment, we observed approximately a 21% reduction in infections. The optimal control for this simulation followed the same behavior as that of the first

time period (T1). For both instances, the optimal control value came out to be u=0.8, where the cost of the first instance of control was 3854 and the cost of the second instance of control was 4411. Overall, this simulation was similar to that of the first time period such that both of these simulations showcased an increase in cost for maintaining the current control value.

4. CONCLUSIONS

We presented a Nonlinear Model Predictive Control (NMPC) approach to the mitigation of epidemic spread. Our underlying epidemiological model is an SLIR framework wherein the spatio-temporal spread dynamics is represented using a system of coupled, reaction-diffusion type, partial differential equations. Building upon this dynamic model, we applied the NMPC approach to COVID-19 data for Hamilton County, Ohio, USA. The application of control followed a uniformly implemented control scheme across the entire spatial domain. Spatio-temporal reductions in new infections (i.e. the spread) corresponding to this control scheme were quantitatively analyzed while accounting for the cost of the control measures in each case. Specifically, for the periods T1, T2, and T3 investigated, both the first and third periods witnessed the application of a minimum amount of control. While the second time period implemented control with quantitatively medium intensity. Ultimately, for all three time periods they each experienced control uniformly across the domain and with respect to the infection trends for these time periods the optimized NPI control actions are shown to provide increased mitigation of the epidemics spread.

We note that, to the best of our knowledge, this is one of the first research efforts to develop an NMPC framework for mitigation of epidemics using a PDE-based SLIR model. Indeed, the results suggest several directions for future work. The use of nonlinear PDEs within MPC frameworks is itself largely unexplored, and there are interesting theoretical merits in exploring approaches based on linearization as well as rigorous PDE to ODE conversions. Additionally, in the context of epidemic mitigation, obtaining accurate representations of NPIs in the SLIR model is also a noteworthy future direction of work where a variety of mechanistic or data-driven approaches can be explored. Expanding the uniform control scheme to consider a targeted/selective control scheme based on geographical areas also merits interest. Finally, obtaining an accurate representation of the socioeconomic impacts of the NPI measures is another challenging yet potentially rewarding area of potential future work. We conclude with the hope that the results presented in this article motivate further research.

REFERENCES

Armaou, A., Katch, B., Russo, L., and Siettos, C. (2022). Designing social distancing policies for the COVID-19 pandemic: A probabilistic model predictive control approach. *MBE*, 19(9), 8804–8832.

Atangana, A. and İgret Araz, S. (2022). Fractional Stochastic Differential Equations: Applications to COVID-19 Modeling. Industrial and Applied Mathematics. Springer Nature Singapore, Singapore.

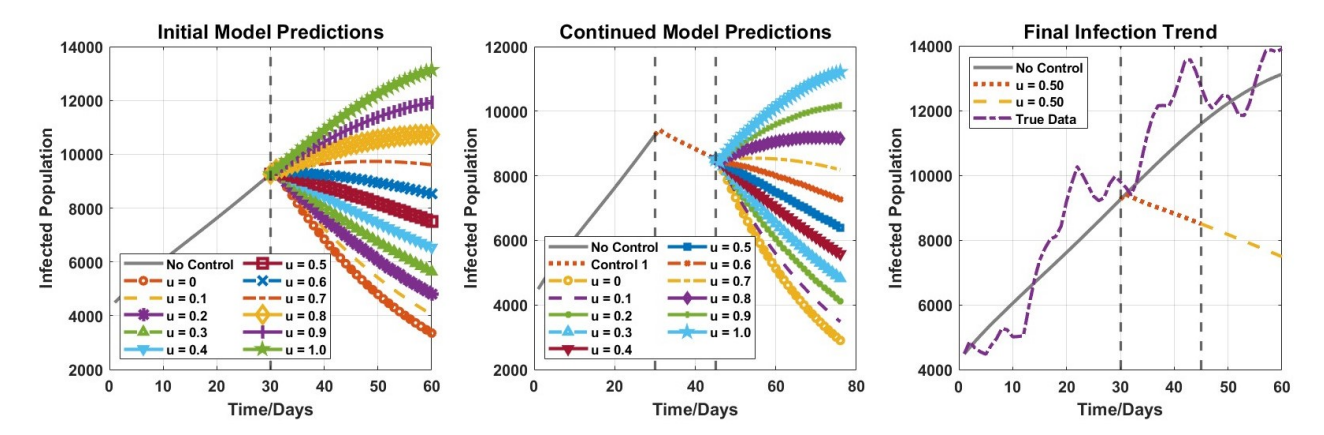


Fig. 2. NMPC (T2) Simulation Process

Carli, R., Cavone, G., Epicoco, N., Scarabaggio, P., and Dotoli, M. (2020). Model predictive control to mitigate the COVID-19 outbreak in a multi-region scenario. *Annual Reviews in Control*, 50, 373–393.

CDC (2023). David J. Sencer CDC Museum COVID-19 Timeline. Publication Title: Centers for Disease Control and Prevention Type: Government.

Deshpande, A., Kumar, M., and Ramakrishnan, S. (2017). Robot Swarm for Efficient Area Coverage Inspired by Ant Foraging: The Case of Adaptive Switching Between Brownian Motion and Lévy Flight. In ASME 2017 Dynamic Systems and Control Conference. American Society of Mechanical Engineers.

Dietze, S. and Grepl, M.A. (2023). Reduced order model predictive control for parametrized parabolic partial differential equations. Applied Mathematics and Computation, 453, 128044.

Dufour, P., Michaud, D., Touré, Y., and Dhurjati, P. (2004). A partial differential equation model predictive control strategy: application to autoclave composite processing. *Computers & Chemical Engineering*, 28(4), 545–556.

Köhler, J., Schwenkel, L., Koch, A., Berberich, J., Pauli, P., and Allgöwer, F. (2021). Robust and optimal predictive control of the COVID-19 outbreak. *Annual Reviews in Control*, 51, 525–539.

Majid, F., Deshpande, A.M., Ramakrishnan, S., Ehrlich, S., and Kumar, M. (2021). Analysis of epidemic spread dynamics using a PDE model and COVID-19 data from Hamilton County OH USA. *IFAC-PapersOnLine*, 54(20), 322–327.

Majid, F., Gray, M., Deshpande, A.M., Ramakrishnan, S., Kumar, M., and Ehrlich, S. (2022). Non-Pharmaceutical Interventions as Controls to mitigate the spread of epidemics: An analysis using a spatiotemporal PDE model and COVID-19 data. *ISA Transactions*, 124, 215-224.

Mandal, M., Jana, S., Nandi, S.K., Khatua, A., Adak, S., and Kar, T. (2020). A model based study on the dynamics of COVID-19: Prediction and control. *Chaos*, *Solitons & Fractals*, 136, 109889.

Maziarz, M. and Zach, M. (2020). Agent-based modelling for SARS-CoV-2 epidemic prediction and intervention assessment: A methodological appraisal. *Evaluation Clinical Practice*, 26(5), 1352–1360.

Mehta, M., Julaiti, J., Griffin, P., and Kumara, S. (2020).
Early Stage Machine Learning-Based Prediction of US County Vulnerability to the COVID-19 Pandemic: Machine Learning Approach. JMIR Public Health Surveill, 6(3), e19446.

Morato, M.M., Pataro, I.M., Americano Da Costa, M.V., and Normey-Rico, J.E. (2022). A parametrized nonlinear predictive control strategy for relaxing COVID-19 social distancing measures in Brazil. *ISA Transactions*, 124, 197–214.

Scarabaggio, P., Carli, R., Cavone, G., Epicoco, N., and Dotoli, M. (2022). Nonpharmaceutical stochastic optimal control strategies to mitigate the covid-19 spread. *IEEE Trans. Automat. Sci. Eng.*, 19(2), 560–575.

Shamil, M.S., Farheen, F., Ibtehaz, N., Khan, I.M., and Rahman, M.S. (2021). An Agent-Based Modeling of COVID-19: Validation, Analysis, and Recommendations. *Cogn Comput.*

Torlapati, J. and Clement, T.P. (2019). Using Parallel Genetic Algorithms for Estimating Model Parameters in Complex Reactive Transport Problems. *Processes*, 7(10), 640.

Truszkowska, A., Behring, B., Hasanyan, J., Zino, L., Butail, S., Caroppo, E., Jiang, Z., Rizzo, A., and Porfiri, M. (2021). COVID-19 Modeling: High-Resolution Agent-Based Modeling of COVID-19 Spreading in a Small Town (Adv. Theory Simul. 3/2021). Advcd Theory and Sims, 4(3), 2170005.

Wang, H. and Yamamoto, N. (2020). Using a partial differential equation with Google Mobility data to predict COVID-19 in Arizona. *Mathematical Biosciences and Engineering*, 17(5), 4891–4904.

Wang, W., Cai, Y., Wu, M., Wang, K., and Li, Z. (2012). Complex dynamics of a reaction-diffusion epidemic model. *Nonlinear Analysis: Real World Applications*, 13(5), 2240–2258.

Yang, W., Karspeck, A., and Shaman, J. (2014). Comparison of Filtering Methods for the Modeling and Retrospective Forecasting of Influenza Epidemics. *PLoS Comput Biol*, 10(4), e1003583.

Yarsky, P. (2021). Using a genetic algorithm to fit parameters of a COVID-19 SEIR model for US states. Mathematics and Computers in Simulation, 185, 687– 695.